

Detection of atomic force microscopy cantilever displacement with a transmitted electron beam

R. Wagner, T. J. Woehl, R. R. Keller, and J. P. Killgore

Citation: [Applied Physics Letters](#) **109**, 043111 (2016); doi: 10.1063/1.4960192

View online: <http://dx.doi.org/10.1063/1.4960192>

View Table of Contents: <http://scitation.aip.org/content/aip/journal/apl/109/4?ver=pdfcov>

Published by the [AIP Publishing](#)

Articles you may be interested in

[Internal damping for noncontact atomic force microscopy cantilevers](#)

J. Vac. Sci. Technol. B **28**, C4E24 (2010); 10.1116/1.3374736

[Magnetostriction-driven cantilevers for dynamic atomic force microscopy](#)

Appl. Phys. Lett. **95**, 143505 (2009); 10.1063/1.3237180

[Special cantilever geometry for the access of higher oscillation modes in atomic force microscopy](#)

Appl. Phys. Lett. **89**, 033106 (2006); 10.1063/1.2226993

[Optical lever detection in higher eigenmode dynamic atomic force microscopy](#)

Rev. Sci. Instrum. **75**, 5053 (2004); 10.1063/1.1808058

[Theoretical and experimental studies of vibrations of optical fiber cantilevers for atomic force microscopy](#)

Rev. Sci. Instrum. **69**, 1753 (1998); 10.1063/1.1148837

A promotional banner for Applied Physics Reviews. On the left is a small image of a journal cover titled 'AIP Applied Physics Reviews' featuring a diagram of a layered structure. The main text reads 'NEW Special Topic Sections' in large white letters. Below this, it says 'NOW ONLINE' in yellow, followed by 'Lithium Niobate Properties and Applications: Reviews of Emerging Trends' in white. The AIP Applied Physics Reviews logo is in the bottom right corner.

NEW Special Topic Sections

NOW ONLINE
Lithium Niobate Properties and Applications:
Reviews of Emerging Trends

AIP Applied Physics
Reviews

Detection of atomic force microscopy cantilever displacement with a transmitted electron beam

R. Wagner,^{a)} T. J. Woehl,^{a)} R. R. Keller, and J. P. Killgore

Material Measurement Lab, National Institute of Standards and Technology, Boulder, Colorado 80305, USA

(Received 18 April 2016; accepted 20 July 2016; published online 29 July 2016)

The response time of an atomic force microscopy (AFM) cantilever can be decreased by reducing cantilever size; however, the fastest AFM cantilevers are currently nearing the smallest size that can be detected with the conventional optical lever approach. Here, we demonstrate an electron beam detection scheme for measuring AFM cantilever oscillations. The oscillating AFM tip is positioned perpendicular to and in the path of a stationary focused nanometer sized electron beam. As the tip oscillates, the thickness of the material under the electron beam changes, causing a fluctuation in the number of scattered transmitted electrons that are detected. We demonstrate detection of sub-nanometer vibration amplitudes with an electron beam, providing a pathway for dynamic AFM with cantilevers that are orders of magnitude smaller and faster than the current state of the art. [<http://dx.doi.org/10.1063/1.4960192>]

As atomic force microscopy (AFM)¹ transitions from a tool for observing the static nanoscale into one tailored for real time observation of dynamic processes such as molecular motor motion,² protein folding,³ charge transport,⁴ and nanostructure growth,⁵ a series of cascading bottlenecks must be overcome to continue to improve imaging speed. Chief among these bottlenecks is the response time of the AFM cantilever, which is inversely proportional to the cantilever resonance frequency ω . The value of ω is proportional to the square root of the ratio of cantilever stiffness k to cantilever mass m . Thus, improved response time can be achieved by increasing k , which is undesirable for delicate samples, or by decreasing m . Substituting geometric parameters of a rectangular cantilever and isotropic material properties for k and m gives

$$\omega \propto \sqrt{\frac{k}{m}} \propto \frac{h}{L^2} \sqrt{\frac{E}{\rho}}, \quad (1)$$

where h is the cantilever thickness, L is the cantilever length, E is the cantilever Young's modulus, and ρ is the cantilever material density.⁶ For a rectangular cantilever, k is related to geometric parameters and material properties by

$$k = \frac{Eb}{4} \left(\frac{h}{L}\right)^3, \quad (2)$$

where b is the width of the AFM cantilever. These equations show that by decreasing L while holding h/L constant, ω can be increased while k remains constant. This approach has brought the resonance frequency of AFM cantilevers from the tens to hundreds of kHz range into the several MHz range by reducing length from hundreds to tens of micrometers.⁷ By reducing cantilever lengths to sub-micrometer dimensions, further orders of magnitude improvement in speed is possible.

Improved detection schemes are required to accommodate smaller cantilevers. The cantilever position is most

commonly measured by the “optical lever” scheme,⁸ where a focused laser beam is reflected off the cantilever onto a quadrant photodetector. The state of the art optical lever systems for small, fast AFM cantilevers have pushed the spot size of this laser beam close to its practical limit ($\sim 1 \mu\text{m}$). At this limit, the laser spot is contained within the back of the cantilever, without excessive spill-over of light. Other optical methods such as interferometric⁹ and scattering based detection^{10–12} can scale cantilever size down to near the optical diffraction limit ($\sim 200 \text{ nm}$). Alternately, self-sensing technologies such as optomechanical sensors¹³ or piezoelectric sensors^{14,15} allow scaling to smaller sizes at the cost of complicated fabrication and limitations with respect to stiffness. Our proposed solution is to use an electron beam to detect the motion of the AFM cantilever. An electron beam can be focused into a spot size ~ 100 times smaller than an optical beam, enabling the use of much smaller and faster AFM cantilevers.

To demonstrate electron beam detection of cantilever vibrations, an AFM cantilever (NCL, Nanosensors, Germany¹⁶) mounted on a holder (Dimension 3000, Digital Instruments, Santa Barbara, CA) containing a piezoelectric actuator was inserted into a field emission scanning electron microscope (FESEM, Leo Gemini 1525, Carl Zeiss AG, Germany) operating at a beam current of 150 pA and an accelerating voltage of 30 kV. At 30 kV, Monte Carlo simulations of electron scattering¹⁷ predict that more than 99% of electrons will be transmitted through a 200 nm thick section of silicon, maximizing the detected signal. For the same conditions, a temperature rise of less than 10^{-3} K is predicted from inelastic scattering,¹⁸ suggesting that local heating of the AFM tip is negligible. The AFM tip was positioned such that it was under the electron beam and perpendicular to the optic axis of the FESEM (Figure 1(a)). The focused electron beam size for this instrument was approximately 3 nm to 5 nm. We performed electron detection with two different detectors: a solid-state silicon diode transmitted electron (TE) detector (KE Developments, Deben, UK) and a scintillator-based backscatter electron detector (Robinson, ETP Semra, Australia). The scintillator backscatter detector was employed as a TE detector by placing it below the sample

^{a)}R. Wagner and T. J. Woehl contributed equally to this work.

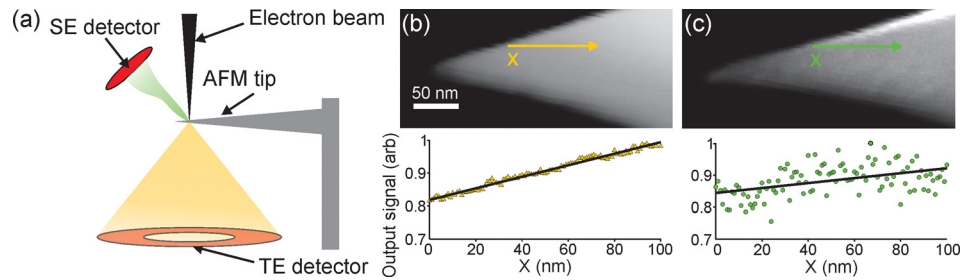


FIG. 1. (a) Schematic of the electron detection scheme for detecting AFM tip position with a focused stationary electron beam and transmitted electron detector. (b) Dark field transmitted electron (TE) and (c) secondary electron (SE) images of a stationary AFM tip. The scatter plots correspond to the normalized image intensities along the green and yellow lines. The black lines are linear least-squares fits. The fit to the TE output signal had a root mean squared error of $RMSE = 0.007$ and goodness of fit $R^2 = 0.983$. The fit parameters for the SE output signal were $RMSE = 0.043$ and $R^2 = 0.22$.

with the active detector area facing up (cf. Figure 1(a)). Both electron detectors were positioned such that they collected scattered transmitted electrons and allowed unscattered electrons to pass through a hole on the optic axis. In this configuration, these detectors produced dark-field (DF) images. The signal used for electron detection of cantilever oscillations was the output video voltage from the electron detector amplifier, which was measured with an oscilloscope (Virtual Bench, National Instruments, Austin, TX, e.g., Figures 2(b) and 3(a)) or a lock-in amplifier (7280, Signal Recovery, Oak Ridge, TN, e.g., Figures 2(c), 3(b), and 3(c)). The output video voltage from the electron detector amplifier, which will be referred to as the output signal, is the voltage conventionally used to form the digital image on the SEM computer and is typically on the order of hundreds of millivolts.¹⁹ Unless otherwise noted, all electron detection data were collected using the output signal from the scintillator TE detector.

The gradient in the material thickness along the length of the AFM tip produces a variation in the output signal that can be used to detect cantilever vibrations. Figure 1(b) shows a DF-TE image of the AFM tip recorded with the solid state silicon diode detector. The plot of the (normalized) DF-TE output signal shows a linear increase of 20% for a 100 nm displacement along the AFM tip (slope of 1.8×10^{-3} , goodness of fit $R^2 = 0.983$). The scintillator TE detector produced similar DF-TE images (cf. Figure 2(a)). The DF-TE image contrast is explained by the mass-thickness contrast mechanism described by

$$\frac{N}{N_0} = 1 - \exp\left(-\frac{T\sigma\rho N_A}{W}\right). \quad (3)$$

Here, N is the number of transmitted electrons scattered to the DF detector by the sample, N_0 is the number of incident electrons, T is the material thickness, σ is the scattering cross section of the material, ρ is the material density, N_A is Avogadro's number, and W is the atomic weight of the material.¹⁹ Figure S1 in the supplementary material²⁰ demonstrates the inverse exponential dependence predicted by Equation (3) for displacements of $\sim 1 \mu\text{m}$ along the AFM tip. The first-order term in the Taylor series expansion of Equation (3) around T is

$$\frac{N}{N_0} \approx \frac{T\sigma\rho N_A}{W}. \quad (4)$$

The ratio, $\frac{N}{N_0}$, is proportional to the detector output signal, with the brightness and contrast of the image as proportionality constants. Given the linear thickness gradient of the AFM tip, the linear relationship observed in Figure 1(b) is reasonable for small changes in the position of the AFM tip relative to the electron beam.

In the SEM, secondary electron (SE) imaging is far more common than TE imaging, inviting a comparison between the detection methods. We compared the output signal obtained with a conventionally-positioned Everhart-Thornley SE detector to that obtained with TE detection. Figure 1(c) shows a representative SE image of the AFM tip, with a corresponding plot of the SE output signal (normalized to the maximum) along the green line in the image. The SE signal increases approximately 5% for a 100 nm displacement along the AFM tip with a fitted slope of 7.75×10^{-4} , albeit with a significant amount of noise and weak linear dependence ($R^2 = 0.22$). The TE image in Figure 1(b) has an

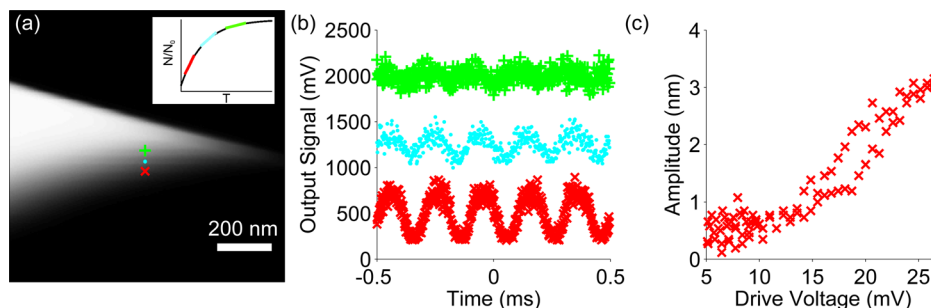


FIG. 2. (a) Dark field transmitted electron image of the AFM tip. The markers in the image correspond to the electron detection locations where the output signal was recorded. (b) Output signal of the electron detector captured with the same drive amplitude (1414 mV) and drive frequency (5 kHz) but at different electron beam locations. The offset of the y-scale has been arbitrarily shifted to clearly show the three cases on a common axis. (c) Plot of amplitude of cantilever displacement versus drive amplitude when the electron beam was near the edge of the tip (red x in (a)) and the drive frequency was 5 kHz.

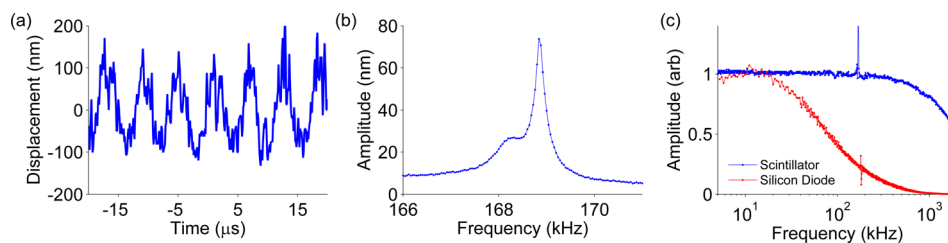


FIG. 3. Response of a vibrating AFM cantilever detected by transmitted electrons. (a) Displacement of the AFM tip at a frequency of 168.85 kHz and a drive amplitude of 141.4 mV. (b) Amplitude of cantilever displacement as the drive frequency was swept through the cantilever resonance at a drive amplitude of 141.4 mV. (c) Normalized amplitude of the output signal during a broad-range frequency sweep for two different electron detectors.

order of magnitude less error in the linear fit compared to the SE image. Based on the linear relationship between the output signal and displacement for small oscillations and the low noise and larger slope relative to SE imaging, we conclude that the TE signal is superior for thickness-based detection of AFM cantilever vibration.

Dynamic AFM operation requires that we detect a vibrating AFM cantilever as opposed to the stationary cantilever shown in Figure 1. To demonstrate this, we acquired a DF-TE image of the AFM tip and used this image to position a stationary electron beam on the tip in “spot mode.” We then provided a sinusoidal drive voltage to the piezoelectric actuator in the cantilever holder and monitored the output signal of the TE detector (see Figure S2²⁰ and supplementary movie 1²⁰ for TE SEM images and movie of AFM tip with and without drive voltage applied). Figures 2(a) and 2(b) show the position of the stationary electron beam and the corresponding output signal for three different detection positions for an AFM cantilever oscillating at 5 kHz with a drive voltage of 1414 mV, which produced a vibration amplitude of approximately 200 nm. The amplitude of the output signal was largest when the electron beam was placed near the edge of the AFM tip (red x, Figures 2(a) and 2(b)) and decreased when the electron beam was placed closer to the center of the tip (blue diamond and green cross, Figures 2(a) and 2(b)). As qualitatively shown in the inset in Figure 2(a), the sensitivity of the output signal to vibrations decreases with increasing material thickness due to the exponential dependence of $\frac{N}{N_0}$ on material thickness (Equation (3) and Figure 2(a) inset). The signal to noise ratio SNR, calculated from the power spectral density of the time domain data in Figure 2(b), improves from 6.9 at the green cross to 18.9 at the blue dot, and to 45.1 at the red x. The improvement in the SNR when moving the electron beam to thinner portions of the tip suggests a pathway towards better SNR by optimizing the geometry of the tip and the position of the beam. Combined with the mass-thickness electron scattering theory, this experiment demonstrates that the absolute material thickness associated with the position of the detecting electron beam determines the sensitivity of the measurement and shows that the placement of the electron beam near the edge of the AFM tip produces the most sensitivity to cantilever oscillations.

Because the electron beam position on the AFM tip can be controlled and the beam has a calibrated position, calibration of the displacement of the AFM tip is possible. To calibrate the relationship between the output signal and cantilever displacement, we scanned the electron beam along

a 200 nm horizontal line near the red x in Figure 2(a) on a stationary AFM tip and measured the output signal with an oscilloscope. From the slope of the output signal and known length of the electron beam scan, we determined the sensitivity of the electron detection near the red x to be (1.3 ± 0.4) mV/nm (all uncertainties are reported to the 95% confidence interval). The detection sensitivity will depend specifically on the location of the beam spot, the electron detector brightness and contrast settings, and the shape and composition of the AFM tip, which can change over time due to carbon buildup and amorphization.¹⁹ The average power spectral density of the calibrated output signal near the red x in the bandwidth of 10 kHz to 250 kHz was measured to be 0.1 nm/ $\sqrt{\text{Hz}}$. This value is higher than that for modern commercial AFM instruments and will need to be reduced to achieve high performance imaging. The noise floor is strongly dependent on the local thickness of the AFM tip and can be improved with optimization of the electron detection system including better positional stability, allowing positioning of the electron beam on thinner portions of the tip.

To better understand the minimum amplitude of the cantilever displacement that could be measured with the electron detection scheme, we continuously increased the amplitude of the drive voltage while the electron beam was positioned near the red x in Figure 2(a) and measured the amplitude of the cantilever displacement with the lock-in amplifier. From the measured sensitivity and the drive amplitude ramp in Figure 2(c), we concluded that with a lock-in time constant of 10 ms the minimum detectable amplitude at a frequency of 5 kHz was 0.9 nm. High-speed imaging will require faster lock-in time constants to coincide with higher pixel acquisition rates. At the current noise levels, increasing the resonance frequency will proportionally decrease the integration time required to average a fixed number of oscillation cycles. The thermal noise limit will also be improved with higher frequency cantilevers because the noise is distributed over a wider frequency band.⁶ Furthermore, by improving the SNR in the measurement as discussed above, the requisite number of oscillations required for precise amplitude measurement will decrease.

Frequency sweep experiments over the electron detector bandwidth demonstrated the ability to measure the resonant frequency of an AFM cantilever and demonstrated the role of the electron detector bandwidth in limiting the measurable frequency range. Figure 3(a) shows the on-resonance cantilever displacement over several oscillation periods at a drive frequency of 168.85 kHz and a drive amplitude of 141.4 mV. The amplitude of the displacement while the drive frequency

was swept through the cantilever resonance is shown in Figure 3(b). This result demonstrates that the dynamic motion of the AFM cantilever at and near resonance can be detected with the TE electron signal. Observation of this resonance peak confirms that the output signal is not the product of a stray electric field from driving the piezoelectric actuator because this resonance peak is a property of the mechanical motion of the AFM cantilever. Figure 3(c) compares the normalized amplitude of the scintillator and silicon diode detector output signals for long range frequency sweeps on two different cantilevers of the same type. The scintillator detector had a cut off frequency (3dB bandwidth) of (1300 ± 20) kHz and the silicon diode detector had a cut off frequency of (43 ± 2) kHz. Therefore, for the specific detectors used in these experiments, the scintillator detector is better for higher frequency measurements. Nonetheless, the scintillator detector is still not operating close to its theoretical response time, which is reported to be on the order of nanoseconds.¹⁹ This suggests that post-detector electronics were responsible for the roll off observed in Figure 3(c). An optimized detector for this technique will have faster post-detector electronics allowing for higher detector cut off frequencies.

For AFM applications employing electron beam detection, consideration must be given to sample limitations. Both sample roughness and sample tilt may affect the ability of the electron beam to access the tip in a side-illumination configuration. Substrates will have to be smooth, and relative sample and beam tilt will have to be carefully adjusted in the SEM. This concern could be partially alleviated by placing a separate tip for electron detection on the backside of the cantilever, further from the sample surface. A second sample consideration is the interaction between the scattered electrons and fragile specimens. A Monte Carlo simulation¹⁷ (see Figure S3 in the supplementary material²⁰) of electron scattering through a 150 nm thick section of the tip indicated that fewer than 0.1% of transmitted electrons scattered to angles greater than 60° (where 90° represents the sample directly beneath the tip). This suggests that a sample area on the order of hundreds of nanometers in diameter surrounding the tip-sample contact point, which would include the scan area, is shadowed and protected from electron irradiation due to the scattering angles of the transmitted electrons.

Additional aspects of this detection scheme must improve before it is practical to implement as part of an AFM system. Spatial drift of the AFM tip relative to the electron beam limited the duration of measurements to ~ 20 s, which is long compared to HS-AFM imaging rates, but still begs improvement. Specimen drift in the SEM is associated with buildup of positive charge in poorly conducting samples irradiated with an electron beam, SEM stage stability, thermal variations due to cooling water cycling, and other factors.¹⁹ A final consideration is that the response time of the AFM cantilever is related to both resonance frequency and quality factor.²¹ The quality factor of a cantilever is typically much higher in vacuum than in air due to a lack of environmental damping; an optimized system would either have a cantilever with a high value of internal damping, an electron detection setup that works at elevated

pressure, or use active quality factor control²² to reduce the quality factor.

We have demonstrated the detection of AFM cantilever vibrations with transmitted electrons in an SEM. We proposed a calibration scheme to relate electron detector output to absolute displacement of the tip. Electron scattering theory and experiments using different electron beam detection positions on the AFM tip showed that the sensitivity of the detection method increased with decreasing material thickness. With this fundamental understanding of the scattering mechanism, we achieved a minimum detectable amplitude of 0.9 nm with an electron beam position near the edge of the AFM tip. Long-range frequency sweeps indicated that the scintillator detector used had a maximum operating frequency of 1300 kHz. Further optimization of the AFM tip stability and electron detection system are pathways to improve both of these metrics. The advantage of the electron detection scheme is the downward scalability of cantilever size by two orders of magnitude. Smaller AFM cantilevers are inherently faster and can retain low stiffness necessary to measure fragile samples. This detection approach is an enabling technology for high speed AFM experiments orders of magnitude faster than the current state of the art.

This work was performed while Ryan Wagner and Taylor Woehl held National Research Council Associateship Awards at NIST. Contribution of NIST, an agency of the U.S. government; not subject to copyright in the United States.

¹G. Binnig, C. F. Quate, and C. Gerber, *Phys. Rev. Lett.* **56**(9), 930–933 (1986).

²M. Schliwa and G. Woehlke, *Nature* **422**(6933), 759–765 (2003).

³A. Borgia, P. M. Williams, and J. Clarke, *Annu. Rev. Biochem.* **77**(1), 101–125 (2008).

⁴Y. Shirota and H. Kageyama, *Chem. Rev.* **107**(4), 953–1010 (2007).

⁵P. Jensen, *Rev. Mod. Phys.* **71**(5), 1695–1735 (1999).

⁶D. A. Walters, J. P. Cleveland, N. H. Thomson, P. K. Hansma, M. A. Wendman, G. Gurley, and V. Elings, *Rev. Sci. Instrum.* **67**(10), 3583–3590 (1996).

⁷T. Ando, T. Uchihashi, and N. Kodera, *Annu. Rev. Biophys.* **42**(1), 393–414 (2013).

⁸S. Alexander, L. Hellemans, O. Marti, J. Schneir, V. Elings, P. K. Hansma, M. Longmire, and J. Gurley, *J. Appl. Phys.* **65**(1), 164–167 (1989).

⁹B. B. Laura, C. T. Ryan, R. Arvind, G. R. Ronald, M. Y. Mehdi, and W. C. Robert, *Nanotechnology* **21**(30), 305701 (2010).

¹⁰G. M. King, A. R. Carter, A. B. Churnside, L. S. Eberle, and T. T. Perkins, *Nano Lett.* **9**(4), 1451–1456 (2009).

¹¹M. Antognozzi, A. Ulcinas, L. Picco, S. H. Simpson, P. J. Heard, M. D. Szczelkun, B. Brenner, and M. J. Miles, *Nanotechnology* **19**(38), 384002 (2008).

¹²B. Sani and P. D. Ashby, *Phys. Rev. Lett.* **104**(14), 147203 (2010).

¹³J. Zou, M. Davanco, Y. Liu, T. Michels, K. Srinivasan, and V. Aksyuk, in *Nanocantilever Beams: Modeling, Fabrication and Applications*, edited by I. Voiculescu and M. Zaghoul (Pan Stanford, 2015).

¹⁴M. Tortonesi, R. C. Barrett, and C. F. Quate, *Appl. Phys. Lett.* **62**(8), 834–836 (1993).

¹⁵M. Li, H. X. Tang, and M. L. Roukes, *Nat. Nanotechnol.* **2**(2), 114–120 (2007).

¹⁶Certain commercial equipment, instruments, or materials are identified in this paper to foster understanding. Such identification does not imply recommendation or endorsement by the National Institute of Standards and Technology, nor does it imply that the materials or equipment identified are necessarily the best available for the purpose.

¹⁷H. Demers, N. Poirier-Demers, A. R. Couture, D. Joly, M. Guilmain, N. de Jonge, and D. Drouin, *Scanning* **33**(3), 135–146 (2011).

¹⁸R. F. Egerton, P. Li, and M. Malac, *Micron* **35**(6), 399–409 (2004).

¹⁹L. Reimer and H. Kohl, *Transmission Electron Microscopy: Physics of Image Formation* (Springer, New York, 2008).

²⁰See supplementary material at <http://dx.doi.org/10.1063/1.4960192> for additional figures.

²¹J. D. Adams, B. W. Erickson, J. Grossenbacher, J. Brugger, A. Nievergelt, and G. E. Fantner, *Nat. Nanotechnol.* **11**(2), 147–151 (2016).

²²T. Sulchek, R. Hsieh, J. D. Adams, G. G. Yaralioglu, S. C. Minne, C. F. Quate, J. P. Cleveland, A. Atalar, and D. M. Adderton, *Appl. Phys. Lett.* **76**(11), 1473–1475 (2000).